Journal of Solid Mechanics Vol. 14, No. 3 (2022) pp. 361-376
DOI: 10.22034/jsm.2021.1929863.1695

Research Paper

Analytical Study on the Effect of Stacking Sequence on the Maximum Allowable Heat Flux in Perforated Symmetric Composite Laminates Subjected to Uniform Heat Flux

M.H. Bayati Chaleshtari [1], H. Khoramishad [1,*] , M. Jafari[2]

[1] *Adhesively Bonded and Sandwich Structures Research Laboratory, School of Mechanical Engineering, Iran University of Science and Technology, Tehran, Iran*
[2] *Department of Mechanical Engineering, Shahrood University of Technology, Shahrood, Iran*

Received 2 June 2022; accepted 5 August 2022

ABSTRACT

An analytical solution was used for obtaining the maximum allowable heat flux in symmetric composite laminates containing a quasi-square cutout with different stacking sequences subjected to uniform heat flux. The Tsai-Hill criterion was used to assess the maximum allowable heat flux of the laminate. The analytical solution was obtained based on the thermoelasticity theory and the Lekhnitskii's method. Furthermore, by employing a suitable mapping function, the solution of symmetric laminates with a circular cutout was extended to the quasi-square cutout. The quasi-square cutout was studied in a symmetric laminate made of Glass/epoxy with different stacking sequences of $[0/90]_S$, $[45/-45]_S$, $[30/-30]_S$. The results showed that the maximum allowable heat flux experienced in perforated plates can be improved by considering the appropriate stacking sequence and the optimal values of the cutout parameters. According to the results, the best cutout geometry was not always a circle, as in some cases by choosing the appropriate values of bluntness parameter, cutout orientation, heat flux angle, cutout aspect ratio and laminate stacking sequence, a non-circular cutout provided higher maximum allowable heat flux value for a perforated plate than a circular cutout.

Keywords : Stacking sequence; Maximum allowable heat flux; Cutout orientation angle; Heat flux angle; Quasi-squared cutout; Complex variable method.

1 INTRODUCTION

POLYMERIC composites are being extensively used in various industries. In order to adapt composite laminates for engineering applications, cutouts may be introduced into the structures [1,2]. However, the presence of cutouts in structures can lead to strength reduction and consequent premature structural failure [3].

*Corresponding author. Tel.: +98 77240540; Fax.: +98 77240540.
E-mail address: khoramishad@iust.ac.ir (H. Khoramishad)

Therefore, it is of high importance that the stress concentration and strength reduction due to cutouts are predicted prior to manufacturing for reaching to an acceptable design. One of the service conditions that structures may experience is thermal loading. The stress distribution in perforated plates was studied analytically by many researchers. First, Muskhelishvili [4] and Lekhnitskii [5] used conformal mapping and complex variable method for stress analysis of isotropic and anisotropic plates with a central cutout. Muskhelishvili [4] introduced the complex variable method for stress analysis of isotropic plates. Afterward, Lekhnitskii [5] used an analytical solution for stress analysis of anisotropic plates with circular and elliptical cutouts using the complex variable method based on the Kolosov-Muskhelishvili formulation. Florence and Goodier [6,7] employed the complex variable method in solving the boundary value problems of two-dimensional thermoelasticity. They obtained thermal stresses in an elastic isotropic plate with circular and elliptical cutouts under uniform heat flux. Hasebe [8] derived formulations for two-dimensional thermo-elastic problems. The material properties of the plates were isotropic, homogeneous and linear elastic governed by the Hooke's law. By applying the complex variable method, complex functions were obtained for various thermal and mechanical conditions. Tarn and Wang [9] extended the Lekhnitskii's complex variable method and obtained thermal stresses in an anisotropic elastic plate with a circular cutout or a rigid inclusion by assuming plane strain and stress conditions. Rezaeepazhand and Jafari [10] utilized the Lekhnitskii's complex variable method to analyze stresses in composite plates with a central cutout. Then, Jafari and Bayati [11] applied the metaheuristic algorithms to optimum stresses in composite plates with a central cutout. Parametric studies were conducted to examine the effects of the material properties and the cutout bluntness and orientation for the circular, triangular and square shaped-cutouts on the location and the value of the maximum stress in a flat composite plate subjected to uniaxial tension load. The stacking sequence of laminated composites is an important parameter to determine the strength of the plate under different load such as buckling loading [12], fatigue loading [13], mechanical loading [14,15], thermal loading [16]. Ukadgaonker and Rao [17] employed a complex variable technique to determine the mechanical stress distribution around various cutouts in symmetric laminates. The orientation angle and the stacking sequence were the important parameters they studied. Sharma [18] obtained a general solution based on the complex variable method to determine stresses around a non-circular cutout in a laminated composite infinite plate subjected to arbitrary biaxial loading, with layers of arbitrary fiber orientations and stacking sequences. Sharma [19] examined the effect of cutout geometrical parameters on stress distribution in infinite isotropic plates under in-plane loading. A complex variable technique and conformal transformation were employed to determine the mechanical stress distribution around various cutouts in isotropic plates. Sarvestani et al. [20] proposed an analytical method to determine the inter-laminar stresses in symmetric laminated composite plates subjected to shear loading. Moreover, they employed the first-order shear deformation theory and Reddy's layer-wise theory to determine the inter-laminar stresses in composite laminates under tension load with various stacking sequence. Zhou et al. [21] presented an analytical solution to determine the thermoelectric behavior of materials in an infinite plate with a circular cutout subjected to a uniform heat flux. They used the complex variable method and mapping function to obtain the stress concentration around the cutout. Kaczynski [22] employed an analytical method to investigate thermal stresses in a transversely isotropic plate with insulated inclusion under a uniform heat flux. Dave and sharma [23] examined the stress distribution around a square cutout in a functionally graded plate under mechanical loading. Rasouli and jafari [24] applied conformal mapping technique and extended the Lekhnitskii's method to obtain the thermal stress values around circular and elliptical cutouts in an anisotropic plate subjected to a uniform heat flux. The effect of cutout orientation and flux angle as significant parameters was examined on stress distribution. Chao et al. [25] introduced a new analytical solution based on the complex variable method to determine the stress distribution around two circular inclusions in an infinite plate under remote uniform heat flux. Chao and Gao [26] applied the Lekhnitskii's method to provide general analytical solution for an infinite anisotropic laminate containing an elliptical inclusion subjected to uniform heat flux. Chaudhuri and Seide [27,28] obtained the transverse shear stresses around elliptical cutout and inter-laminar shear stresses around the circular cutout in an edge loaded laminated composite plate by applying the equilibrium compatibility method. Rao et al. [29] used Tsai-Hill, Hashin-Rotem and Tsai-Wu criteria to determine the failure strength of a symmetric composite laminate containing a square cutout with various stacking sequence under in-plane loading. They used complex variable formulation and mapping function to obtain the stress concentration around the cutout. Zhou et al. [30,31] examined the fiber and matrix damages in a multilayer composite plate with cutout based on the Tsai-Wu and Hoffman failure criteria under mechanical loading. Patel and Sharma [32] applied an analytical solution based on the complex variable method for obtaining the optimum stacking sequence in a composite laminate with triangular and square cutouts subjected to in-plane loading. They analyzed failure strength using Tsai-Hill criterion. Zhou et al. [33] studied the effect of different stacking sequences of composite laminates with a cutout on the failure of laminates under tensile loading by finite element and analytical methods. Sharma et al. [34] obtained the optimum value of stress concentration factor in a symmetric multilayer composite with an elliptical cutout subjected to

mechanical loading. They used complex variable method and Tsai–Hill criterion to achieve the failure strength of the laminate with different stacking sequence. Jafari et al. [35] used an analytical solution based on the complex variable technique to minimize the stress in a symmetric composite laminate with a polygonal cutout under mechanical loading. They applied Tsai-Hill criterion for investigating the failure strength of the laminate with different stacking sequence. Furthermore, the distribution of stress and displacement over the square cutout in an orthotropic infinite plate under uniform heat flux was examined by Jafari [36].

The purpose of this paper is investigating the effect of stacking sequence on the maximum allowable heat flux in a symmetric composite laminate with a quasi-square cutout under uniform heat flux using an analytical solution based on the complex variable method, the mapping function and the Tsai-Hill criterion. The symmetric Glass/epoxy laminates with different stacking sequences containing a quasi-square cutout were studied analytically. The effect of the heat flux angle and different geometrical parameters of cutout were studied on the thermal stresses and allowable heat flux.

2 THEORETICAL FORMULATIONS

The symmetric composite laminates considered in this study was assumed to be linear elastic and anisotropic governed by the generalized Hooke's law. The edges of the quasi-square cutout were thermally insulated. The size of cutout in comparison with the dimensions of the laminate was small enough for assuming infinite laminate. The cutout angular position represented by β indicates its orientation relative to the horizontal axis. As shown in Fig. 1, the laminate was subjected to a remote uniform heat flux q in steady state condition.

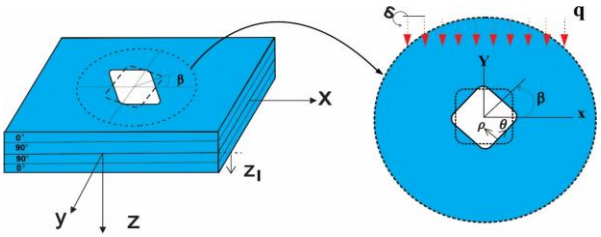

Fig.1
Symmetric composite laminate containing quasi-square cutout under uniform heat flux.

The uniform heat flux was disturbed by the presence of a thermally insulated quasi-square cutout giving rise to thermal stresses around the cutout. Due to the absence of heat source in the laminate, the maximum stress occurred on the edges of the cutout. Moreover, because of the boundary conditions around the cutout, the only stress induced on the edges of cutout was σ_θ by considering the normal and tangential coordinate system (ρ,θ) according to Fig. 1. The plane stress condition and small deformation were assumed. The thermal stress components can be obtained using Eq. (1) [37].

$$\{\sigma\}^T = \{\Phi\}.\Delta T \tag{1}$$

In which

$$\begin{Bmatrix} \Phi_x \\ \Phi_y \\ \Phi_{xy} \end{Bmatrix} = \frac{1}{H}\sum_{l=1}^{N} \begin{bmatrix} \bar{Q}_{11} & \bar{Q}_{12} & \bar{Q}_{16} \\ \bar{Q}_{12} & \bar{Q}_{22} & \bar{Q}_{26} \\ \bar{Q}_{16} & \bar{Q}_{26} & \bar{Q}_{66} \end{bmatrix}^l \begin{Bmatrix} \overline{\alpha_x} \\ \overline{\alpha_y} \\ \overline{\alpha_{xy}} \end{Bmatrix}^l (z_l - z_{l-1}) \tag{2}$$

where ΔT is temperature gradient, z_l and z_{l-1} represent the z components of the upper and lower boundaries of the l^{th} layer, H is the total thickness and $\{\bar{\alpha}\}^l$ is the vector of the coefficient of thermal expansion of the l^{th} layer that is determined using Eq. (3).

$$\overline{\alpha_x} = \alpha_{11}m^2 + \alpha_{22}n^2 \qquad \overline{\alpha_y} = \alpha_{11}n^2 + \alpha_{22}m^2 \qquad \overline{\alpha_{xy}} = 2mn(\alpha_{11} - \alpha_{22}) \tag{3}$$

where α_{11} and α_{22} are the coefficients of thermal expansion in the principle material coordinate system. Furthermore, m and n are the corresponding cosine and sine of the fiber angle (γ). The stress components are defined as Eq. (4) by considering the Airy's stress function $E(x,y)$ [4].

$$\sigma_x = \frac{\partial^2 E}{\partial y^2}, \quad \sigma_y = \frac{\partial^2 E}{\partial x^2}, \quad \tau_{xy} = -\frac{\partial^2 E}{\partial x \partial y} \tag{4}$$

According to the Likhnitskii's complex potential technique, using Eqs. (1) and (4) and the stress-strain relationship and the compatibility equation, the constitutive equation for an anisotropic material can be obtained in terms of the stress function as Eq. (5).

$$\begin{aligned} &a_{11}\frac{\partial^4 E}{\partial y^4} - 2a_{16}\frac{\partial^4 E}{\partial x \partial y^3} + (2a_{12} + a_{66})\frac{\partial^4 E}{\partial x^2 \partial y^2} - 2a_{26}\frac{\partial^4 E}{\partial x^3 \partial y} + a_{22}\frac{\partial^4 E}{\partial x^4} \\ &= -\alpha_x \frac{\partial^2 T}{\partial y^2} + \alpha_{xy}\frac{\partial^2 T}{\partial x \partial y} - \alpha_y \frac{\partial^2 T}{\partial x^2} \end{aligned} \tag{5}$$

where α_x, α_y and α_{xy} are the coefficients of thermal expansion of the laminate and a_{ij} are the coefficients of the reduced compliance matrix [35]. The solution of Eq.(5) is divided into two parts including the homogenous part ($E^{(h)}$) and the particular part ($E^{(p)}$). The generalized biharmonic equation for an anisotropic material in terms of the stress function (E) is:

$$a_{11}\frac{\partial^4 E^{(h)}}{\partial y^4} - 2a_{16}\frac{\partial^4 E^{(h)}}{\partial x \partial y^3} + (2a_{12} + a_{66})\frac{\partial^4 E^{(h)}}{\partial x^2 \partial y^2} - 2a_{26}\frac{\partial^4 E^{(h)}}{\partial x^3 \partial y} + a_{22}\frac{\partial^4 E^{(h)}}{\partial x^4} = 0 \tag{6}$$

Using four first-order linear differential operators $D_k = \frac{\partial}{\partial y} - s_k \frac{\partial}{\partial x}$, in which s_k (k=1,2,3,4) are the roots of Eq. (7), Eq. (6) can be rewritten as $D_1 D_2 D_3 D_4 E^{(h)} = 0$ [5].

$$a_{11}s^4 - 2a_{16}s^3 + (2a_{12} + a_{66})s^2 - 2a_{26}s + a_{22} = 0 \tag{7}$$

The roots of Eq. (7) can be considered as Eq. (8).

$$\begin{aligned} &s_1 = \alpha_1 + i\beta_1, \quad s_2 = \overline{s_1} = \alpha_1 - i\beta_1 \\ &s_3 = \alpha_2 + i\beta_2, \quad s_4 = \overline{s_3} = \alpha_2 - i\beta_2 \end{aligned} \tag{8}$$

where α_1, α_2 , β_1 and β_2 are real numbers. For symmetric laminates, $a_{16} = a_{26} = 0$. Given the roots of the characteristic equation, the Airy's stress function E in Eq. (4) can be represented as Eq. (9) [9].

$$E = E_1(Z_1) + E_2(Z_2) + \overline{E_1(Z_1)} + \overline{E_2(Z_2)} + E^{(p)} \tag{9}$$

where $Z_k = x + s_k y$ (k=1,2). In Eq. (9), E_1 and E_2 are analytic functions and $\overline{E_1}$ and $\overline{E_2}$ are their conjugates. The new stress function (ψ) is derived using the stress function E as below:

$$\frac{dE}{dz} = \psi_1(Z_1) + \psi_2(Z_2) + \overline{\psi_1(Z_1)} + \overline{\psi_2(Z_2)} + \psi^{(p)} \tag{10}$$

By substituting Eqs. (9) and (10) into Eq. (4), the stress components are determined as Eq. (11).

$$\sigma_x = 2\,Re\left\{s_1^2\psi_1'(Z_1)+s_2^2\psi_2'(Z_2)\right\}+\frac{\partial^2 E^{(p)}}{\partial y^2}$$
$$\sigma_y = 2\,Re\left\{\psi_1'(Z_1)+\psi_2'(Z_2)\right\}+\frac{\partial^2 E^{(p)}}{\partial x^2} \tag{11}$$
$$\tau_{xy} = -2\,Re\left\{s_1\psi_1'(Z_1)+s_2\psi_2'(Z_2)\right\}-\frac{\partial^2 E^{(p)}}{\partial x\partial y}$$

In which $\psi_1'(Z_1)$ and $\psi_2'(Z_2)$ are the derivatives of functions $\psi_1(Z_1)$ and $\psi_2(Z_2)$ with respect to Z_1 and Z_2 , respectively. In order to relate the on-axis heat flux q and temperature gradient in an orthotropic laminate, the Fourier's law is employed in the form of Eq. (12) [39].

$$\begin{Bmatrix} q_1 \\ q_2 \\ q_3 \end{Bmatrix} = -\begin{bmatrix} k_{11} & 0 & 0 \\ 0 & k_{22} & 0 \\ 0 & 0 & k_{33} \end{bmatrix} \begin{Bmatrix} \dfrac{\partial T}{\partial x_1} \\ \dfrac{\partial T}{\partial x_2} \\ \dfrac{\partial T}{\partial x_3} \end{Bmatrix} \tag{12}$$

In Eq. (12), $[k]_{on}$ is the on-axis anisotropic thermal conductivity matrix. It is assumed that the unidirectional laminae are transversely isotropic. The Fourier's law of thermal conduction in the global coordinate system can be presented as Eq. (13).

$$\{q\}_{off} = [T(-\gamma)][k]_{on}[T(\gamma)]\{\nabla T\}_{off}$$
$$[T(-\gamma)] = \begin{bmatrix} \cos\gamma & -\sin\gamma & 0 \\ \sin\gamma & \cos\gamma & 0 \\ 0 & 0 & 1 \end{bmatrix} \tag{13}$$

By considering n = sinγ and m = cosγ, the components of the off-axis thermal conductivity matrix $[k]_{off} = [\bar{k}]$ are defined as Eq. (14).

$$\bar{k}_{11} = m^2k_{11}+n^2k_{22} \qquad \bar{k}_{12} = mn(k_{22}-k_{11}) \qquad \bar{k}_{22} = n^2k_{11}+m^2k_{22}$$
$$\bar{k}_{33} = k_{22} \qquad \bar{k}_{13} = 0 \qquad \bar{k}_{23} = 0 \tag{14}$$

By integrating the thermal conductivity coefficients across the laminate thickness, the resultant of thermal conductivity coefficients for a multilayer laminate can be determined using Eq. (15).

$$[K] = \int_{-H/2}^{H/2}[\bar{k}]^l dz = \frac{1}{H}\sum_{l=1}^{N_L}[\bar{k}]^l(z_l - z_{l-1}) \tag{15}$$

In which, l is layer number and $[K]$ is the resultant thermal conductivity matrix and H is the total thickness of the laminate. For a laminate without internal heat source or sink we have [9]:

$$\nabla.q_i = 0 \tag{16}$$

The governing thermal equation for a homogeneous anisotropic material according to Eq. (12) and Eq. (16) can be obtained as Eq. (17). The general solution of Eq. (17) can be considered as $T= E_t(x+s_t y)$ where s_t are the roots of the characteristic Eq. (18) [36].

$$K_x \frac{\partial^2 T}{\partial x^2} + 2K_{xy} \frac{\partial^2 T}{\partial x \partial y} + K_y \frac{\partial^2 T}{\partial y^2} = 0 \tag{17}$$

$$K_y s_t^2 + 2K_{xy} s_t + K_x = 0 \tag{18}$$

The thermal conductivity matrix is invertible and positive definite ($K_x K_y > K_{xy}^2$).Thus, the characteristic Eq. (18) has a pair of conjugate roots, which the roots with positive imaginary part are considered. Therefore, the general solution of Eq. (18) can be introduced as Eq. (19) [9].

$$T = E_t(x + s_t y) + \overline{E_t(x + s_t y)} = 2Re(E_t(x + s_t y)) \tag{19}$$

In which E_t is a complex function. By substituting Eq. (19) into Eq. (5), the particular solution of the stress functions $E^{(p)}$ can be obtained as Eq. (20).

$$E^{(p)} = 2Re(\upsilon E_t(x + s_t y)) \tag{20}$$

So, by substituting Eq. (20) into Eq. (11), the stress components and displacement field are obtained in terms of stress functions as Eq. (21).

$$\begin{aligned}
\sigma_x &= 2Re\left\{s_1^2 \psi_1'(Z_1) + s_2^2 \psi_2'(Z_2)\right\} + 2Re(\chi s_t^2 \psi_t') \\
\sigma_y &= 2Re\left\{\psi_1'(Z_1) + \psi_2'(Z_2)\right\} + 2Re(\chi \psi_t') \\
\tau_{xy} &= -2Re\left\{s_1 \psi_1'(Z_1) + s_2 \psi_2'(Z_2)\right\} - 2Re(\chi s_t \psi_t') \\
u_x &= 2Re\sum_{k=1}^{2} b_k \psi_k + 2Re(b_t \psi_t) \\
u_y &= 2Re\sum_{k=1}^{2} d_k \psi_k + 2Re(d_t \psi_t)
\end{aligned} \tag{21}$$

where

$$\begin{aligned}
&b_k = a_{11} s_k^2 + a_{12} - a_{16} s_k \qquad k = 1,2 \qquad b_t = \chi(a_{11} s_t^2 + a_{12} - a_{16} s_t) + a_x \\
&d_k = a_{12} s_k + \frac{a_{22}}{s_k} - a_{26} \qquad k = 1,2 \qquad d_t = \chi(a_{12} s_t + \frac{a_{22}}{s_t} - a_{26}) + \frac{a_y}{s_t}
\end{aligned} \tag{22}$$

In which x is defined in Eq. (23).

$$\chi = \frac{(-\alpha_y + \alpha_{xy} s_t - \alpha_x s_t^2)}{a_{11} s_t^4 - 2a_{16} s_t^3 + (2a_{12} + a_{66}) s_t^2 - 2a_{26} s_t + a_{22}} \tag{23}$$

2.1 Conformal mapping function

To extend the analytical solution of a circular cutout to a quasi-square cutout, the infinite areas outside the quasi-square cutout is mapped to the outside areas of a unit circle as shown in Fig. 2, [38].

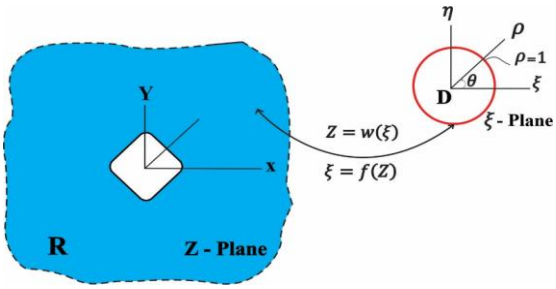

Fig.2
Conformal mapping.

Eq. (24) defines the mapping function used in this study.

$$z_k = w(\xi) = \left[(\cos\theta + w\cos(3\theta)) + s_k(c\sin\theta - w\sin(3\theta))\right] \quad (k = 1,2,t) \tag{24}$$

In which s_k are the roots of the characteristic equation and ξ is defined in Eq. (25) in the mapped plane.

$$\xi = \rho e^{i\theta} = \rho(\cos\theta + i\sin\theta) \tag{25}$$

For a unit circle ρ =1. In Eq. (24), The parameter c determines the aspect ratio of the cutout and w determines the cutout corner curvatures (bluntness parameter). The condition of $0 \le w < 1/n$ ensures that the cutout shape does not have loops. Fig. 3 shows the effect of w on the shape of cutout.

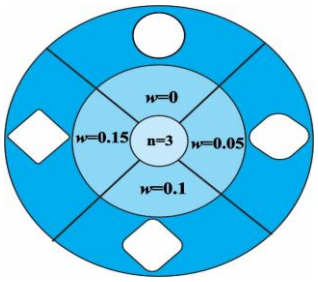

Fig.3
Effect of the parameter w on the shape of cutouts.

Applying the Euler's formula, the conformal mapping function for a quasi-square cutout can be presented as Eq. (26).

$$z_k = w(\xi) = \frac{1}{2}(\Delta_{1k}\xi + \Delta_{2k}\xi^{-1} + \Delta_{3k}\xi^{3} + \Delta_{4k}\xi^{-3}) \tag{26}$$

In which $\Delta_{ik,(i=1,2,3,4)}$ are as below:

$$\begin{aligned} \Delta_{1k} &= \frac{1}{2}[(1 - ics_k)\cos\beta - (ic + s_k)\sin\beta] \qquad \Delta_{3k} = \frac{w}{2}[(1 + is_k)\cos\beta + (i - s_k)\sin\beta] \\ \Delta_{2k} &= \frac{1}{2}[(1 + ics_k)\cos\beta + (ic - s_k)\sin\beta] \qquad \Delta_{4k} = \frac{w}{2}[(1 - is_k)\cos\beta - (i + s_k)\sin\beta] \end{aligned} \tag{27}$$

Eq. (28) is applied to model the cutout angular position (β).

$$\begin{Bmatrix} X \\ Y \end{Bmatrix} = \begin{bmatrix} \cos\beta & \sin\beta \\ -\sin\beta & \cos\beta \end{bmatrix} \begin{Bmatrix} x \\ y \end{Bmatrix} \tag{28}$$

In which x and y represent the Cartesian coordinates in the laminate with quasi-square cutout. It should be noted that β determines the cutout orientation and θ is the angular position around the cutout.

2.2 Boundary condition function

Based on Eq. (21), to achieve the stress components, the stress functions ψ_i and ψ_t need to be determined. For this purpose, the following matrices are defined as Eq. (29) [9].

$$L=\begin{bmatrix}-s_1 & -s_2\\ 1 & 1\end{bmatrix},\qquad l=\begin{bmatrix}-\chi s_t\\ \chi\end{bmatrix},\qquad \psi=\begin{bmatrix}\psi_1\\ \psi_2\end{bmatrix},\quad A^{\wp}=\begin{bmatrix}b_1 & b_2\\ d_1 & d_2\end{bmatrix},\quad a=\begin{bmatrix}b_t\\ d_t\end{bmatrix} \tag{29}$$

The boundary of the quasi-square cutout is free from external load and then the mechanical boundary conditions using Eq. (29) can be rephrasing as Eq. (30).

$$L\psi+\overline{L\psi}+l\psi_t+\overline{l\psi_t}=0 \tag{30}$$

Moreover, because the boundary of the quasi-square cutout is insulated, the Newman boundary condition can be denoted as Eq. (31).

$$\psi_t'(\xi)-\overline{\psi_t'(\xi)}=0 \tag{31}$$

The function $\psi_t'(\xi)$ can be represented by two functions $r_t(\xi)$ and $p_t(\xi)$ that are holomorphic in the inner and outer areas of the unit circle, respectively.

$$\psi_t'(\xi)=r_t(\xi)+p_t(\xi) \tag{32}$$

The function $\psi_t'(\xi)$ can be expressed as the Laurent series in which the term ξ^{-1} exists. Consequently, by integrating the function $\psi_t'(\xi)$, the function $\psi_t(\xi)$ contains the term *log*ξ. Therefore, $\psi_t(\xi)$ is considered as Eq. (33).

$$\psi_t(\xi)=R_t(\xi)+P_t(\xi)+\Upsilon l\log\xi \tag{33}$$

In which $R_t(\xi)$ and $P_t(\xi)$ are holomorphic functions inside and outside the unit circle, respectively. Furthermore, the function $\psi(\xi)$ can be considered as Eq. (34).

$$\psi(\xi)=r(\xi)+p(\xi)+\Lambda l\log\xi \tag{34}$$

where *r(ξ)* and *p(ξ)* are the holomorphic functions inside and outside the unit circle respectively. By substituting Eq. (33) and Eq. (34) into Eq. (30) and multiplying it by $\frac{d\sigma}{2\pi i(\sigma-\xi)}$ and applying the Cauchy integral, $\psi(\xi)$ can be rephrased as Eq. (35).

$$\psi(\xi)=r(\xi)-L^{-1}\bar{L}\bar{r}(\xi^{-1})-L^{-1}lP_t(\xi)-L^{-1}\bar{l}\bar{R}_t(\xi^{-1})+\Lambda\log\xi \tag{35}$$

where

$$\Lambda=L^{-1}(\overline{M}-M)^{-1}(\Upsilon a-\overline{\Upsilon a})+A^{\wp-1}(\overline{M}^{-1}-M^{-1})^{-1}(\Upsilon l-\overline{\Upsilon l})\qquad M=A^{\wp}L^{-1} \tag{36}$$

In which, *L*, *a*, *l* and $A^{\wp}$ are defined in Eq. (29) and Υ can be obtained using boundary conditions. When the heat flux is applied on an anisotropic laminate with no cutout, the thermal stress function is presented as Eq. (37).

$$\psi_t^{\infty\prime} = \frac{q(\cos\delta + \overline{s_t}\sin\delta)}{i(K_x K_y - K_{xy}^2)^{\frac{1}{2}}(s_t - \overline{s_t})}(x + s_t y) \tag{37}$$

In which δ is the heat flux angle. In the presence of a quasi-square cutout, in addition to $\psi_t^{\infty\prime}$, the function $\psi_t^{M\prime}$, which is holomorphic outside the unit circle, is added to the thermal stress function. Therefore, the stress function can be expressed as Eq. (38).

$$\psi_t'(\xi) = \frac{q(\cos\delta + \overline{s_t}\sin\delta)}{i(K_x K_y - K_{xy}^2)^{\frac{1}{2}}(s_t - \overline{s_t})}(\Delta_{1t}\xi + \Delta_{2t}\xi^{-1} + \Delta_{3t}\xi^3 + \Delta_{4t}\xi^{-3}) + \psi_t^{M\prime}(\xi) \tag{38}$$

Δ_{it} are the components of conformal mapping function for a quasi-square cutout. By comparing Eq. (38) and Eq. (32), the function $r_t(\xi)$ is obtained as Eq. (39).

$$r_t(\xi) = \frac{q(\cos\delta + \overline{s_t}\sin\delta)}{i(K_x K_y - K_{xy}^2)^{\frac{1}{2}}(s_t - \overline{s_t})}\left(\Delta_{1t}\xi + \Delta_{3t}\xi^3\right) \tag{39}$$

Therefore, $\psi_t'(\xi)$ is obtained as Eq. (40).

$$\psi_t'(\xi) = \frac{q(\cos\delta + \overline{s_t}\sin\delta)}{i(K_x K_y - K_{xy}^2)^{\frac{1}{2}}(s_t - \overline{s_t})}\left(\Delta_{1t}\xi + \Delta_{3t}\xi^3\right) + \overline{\frac{q(\cos\delta + \overline{s_t}\sin\delta)}{i(K_x K_y - K_{xy}^2)^{\frac{1}{2}}(s_t - \overline{s_t})}\left(\overline{\Delta_{1t}}\xi^{-1} + \overline{\Delta_{3t}}\xi^{-3}\right)} \tag{40}$$

Υ can be obtained by integrating Eq. (40) and comparing it with Eq. (33) as Eq. (41).

$$\begin{aligned}\Upsilon = &-\Delta_{1t}\left(\frac{q(\cos\delta + \overline{s_t}\sin\delta)}{i(K_x K_y - K_{xy}^2)^{\frac{1}{2}}(s_t - \overline{s_t})}\Delta_{2t} - \overline{\frac{q(\cos\delta + \overline{s_t}\sin\delta)}{i(K_x K_y - K_{xy}^2)^{\frac{1}{2}}(s_t - \overline{s_t})}\Delta_{1t}}\right) - \\ &3\Delta_{3t}\left(\frac{q(\cos\delta + \overline{s_t}\sin\delta)}{i(K_x K_y - K_{xy}^2)^{\frac{1}{2}}(s_t - \overline{s_t})}\Delta_{4t} - \overline{\frac{q(\cos\delta + \overline{s_t}\sin\delta)}{i(K_x K_y - K_{xy}^2)^{\frac{1}{2}}(s_t - \overline{s_t})}\Delta_{3t}}\right)\end{aligned} \tag{41}$$

As mentioned, $\psi_t^{\infty\prime}$ expresses the thermal stress function for a laminate with no cutout. Hence, it only causes the laminate deformation and does not create stress. Thus, for the purpose of achieving thermal stresses, $\psi_t^{M\prime}$ should be obtained using Eqs. (37), (38) and (40). The result is presented in Eq. (42).

$$\begin{aligned}\psi_t^{M\prime}(\xi) = &-\left(\frac{q(\cos\delta + \overline{s_t}\sin\delta)}{i(K_x K_y - K_{xy}^2)^{\frac{1}{2}}(s_t - \overline{s_t})}\Delta_{2t} - \overline{\frac{q(\cos\delta + \overline{s_t}\sin\delta)}{i(K_x K_y - K_{xy}^2)^{\frac{1}{2}}(s_t - \overline{s_t})}\Delta_{1t}}\right)\xi^{-1} - \\ &\left(\frac{q(\cos\delta + \overline{s_t}\sin\delta)}{i(K_x K_y - K_{xy}^2)^{\frac{1}{2}}(s_t - \overline{s_t})}\Delta_{4t} - \overline{\frac{q(\cos\delta + \overline{s_t}\sin\delta)}{i(K_x K_y - K_{xy}^2)^{\frac{1}{2}}(s_t - \overline{s_t})}\Delta_{3t}}\right)\xi^{-3}\end{aligned} \tag{42}$$

By comparing Eq. (42) and Eq. (33), the functions $R_t(\xi)$ and $P_t(\xi)$ can be obtained and subsequently by substituting them into Eq. (35), the function $\psi(\xi)$ can be achieved. Finally, the stress components are obtained using Eq. (21).

2.3 Tsai-Hill criterion

In this study the Tsai-Hill criterion (Eq. (43)) is used to determine the allowable heat flux that can be applied on the laminated composite plate with quasi-square cutout. The values of stresses $\sigma_x, \sigma_y, \tau_{xy}$ are transformed into the material principal coordinate in each layer ($\sigma_1, \sigma_2, \tau_6$) and then they are introduced into Eq. (43). The allowable heat flux is determined based on the first ply failure (FPF) scheme [29].

$$Tsai-Hill = (\frac{\sigma_1}{X})^2 + (\frac{\sigma_2}{Y})^2 + (\frac{\tau_6}{S})^2 - \frac{\sigma_1\sigma_2}{X^2} \tag{43}$$

In Eq. (43), X is the tensile strength in longitudinal direction, Y is the tensile strength in transverse direction and S is the shear strength of the unidirectional lamina.

3 VALIDAATION OF THE ANALYTICAL SOLUTION

The ABAQUS finite element code was utilized to validate the proposed analytical solution. The two-dimensional models of Glass/epoxy laminates with quasi-square cutouts under uniform heat flux were developed. The laminates were modeled using the four-noded quadrilateral (S4R) elements. S4R is a general-purpose element, reduced integration with hourglass control, finite membrane strains, and bilinear temperature in the shell surface. A mesh sensitivity analysis was undertaken to ensure the independence of the numerical results to the element size. The region around the cutout was modeled using fine mesh. For the mesh sensitivity analysis, the number of elements was increased from 40 to 360 and it was observed that further refining the mesh did not change the results. Fig. 4 shows the mesh convergence diagram for the Glass/epoxy material with the stacking sequence of $[45/-45]_s$ in and w =0.15, β =30° and δ =270°.

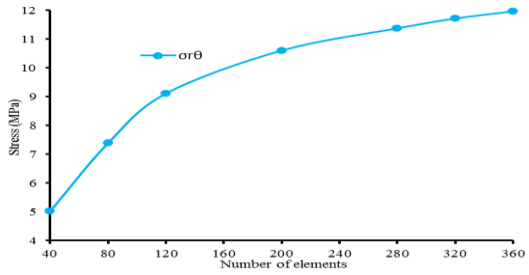

Fig.4
Mesh convergence diagram.

The numerical and analytical stress distributions (σ_θ) around the quasi-square cutout were compared for two different stacking sequences of $[0/90]_s$ and $[45/-45]_s$ in Fig. 5. The parameter θ determines the angular position on the cutout border with respect to the horizontal axis. Fig. 5 indicates reasonable correlation between the numerical and analytical results.

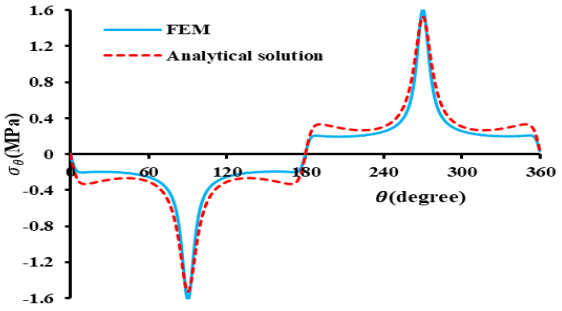

w=0.1, β=0°, c=1, δ=270° with $[0/90]_s$ lay up

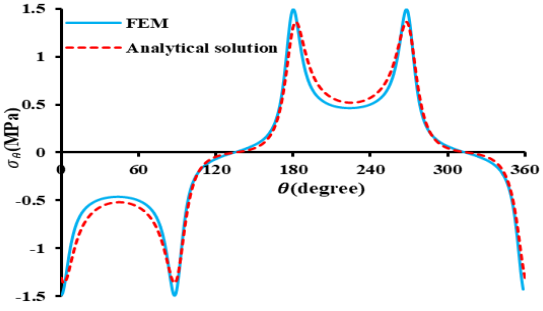

w=0.05, β=45°, c=1, δ=270° with $[45/-45]_s$ lay up

Fig.5
Comparison between the finite element and analytical results.

4 RESULTS AND DISCUSSION

This section presents the maximum allowable heat flux that can be tolerated by the symmetric composite laminates containing a quasi-square cutout under a uniform heat flux. The effect of the cutout bluntness and orientation angle, the heat flux angle, the cutout aspect ratio and the laminate stacking sequence were studied on the maximum allowable heat flux analytically. The laminate studied in this paper was made of Glass/epoxy with the stacking sequences of $[0/90]_s$, $[45/-45]_s$ and $[30/-30]_s$. The laminates were subjected to a uniform heat flux. The Tsai-Hill criterion was used to determine the strengths of the laminates. Note that the default values of the parameters in section 4 are δ =270°, w =0.05, β =0° and c =1, unless the parameter is altered in order to study its effect on the maximum allowable heat flux value. The material properties considered in this study are presented in Table 1.

Table 1
Mechanical properties of the Glass/epoxy material.

Material	$E_{11}(GPa)$	$E_{22}(GPa)$	$G_{12}(GPa)$	υ_{12}	$\alpha_{11}\,(K^{-1})$	$\alpha_{22}\,(K^{-1})$	$X(MPa)$
Glass/epoxy	50	15.2	4.7	0.254	6.34×10^{-6}	2.3×10^{-5}	1000
	$K_{11}\,(Wm^{-1}K^{-1})$		$K_{22}\,(Wm^{-1}K^{-1})$		$Y(MPa)$		$S(MPa)$
	2.2		1.1		30		70
	$E_{33}=E_{22}$, $G_{12}=G_{13}=G_{23}$, $\upsilon_{12}=\upsilon_{13}=\upsilon_{23}$, $\alpha_{33}=\alpha_{22}$, $K_{33}=K_{22}$, $K_{12}=0$						

4.1 Effect of rotation angle of cutout

Fig. 6 shows the maximum allowable heat flux versus the cutout rotation angle (β) for the laminates with different stacking sequences of $[0/90]_s$, $[45/-45]_s$ and $[30/-30]_s$ containing a cutout with different bluntness values (w). As can be seen in Fig. 6, the maximum allowable heat flux value was considerably dependent on the cutout bluntness and rotation angle and the laminate stacking sequence. According to the Tsai-Hill criterion, the maximum allowable heat flux value obtained for the stacking sequence of $[0/90]_s$ was 352 w/m^2 for the cutout rotation angle of β = 45°. Whereas, for the stacking sequences of $[45/-45]_s$ and $[30/-30]_s$, the maximum allowable heat flux values were 456 and 422 w/m^2, respectively for the cutout rotation angles of β = 0° or 90°. Therefore, the highest allowable heat flux value was obtained for the stacking sequence of $[45/-45]_s$. Moreover, it was found out that a laminate with non-circular quasi-square cutout with w = 0.05 tolerated higher allowable heat flux compared to a laminate with circular cutout. Hence, the circular cutout was not the optimum shape for the cutout in the symmetric composite laminate subjected to uniform heat flux.

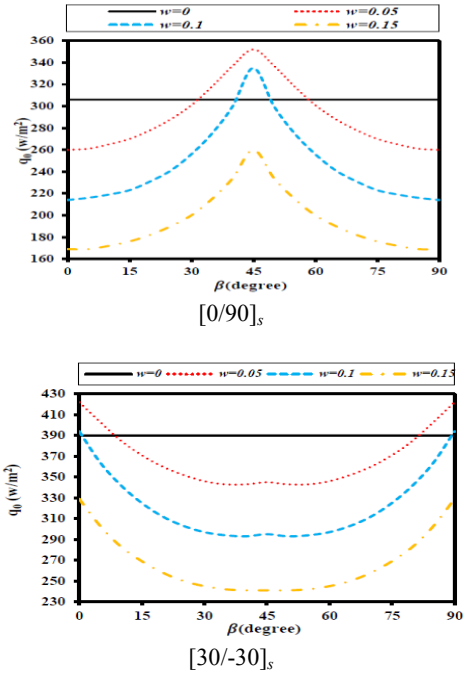

$[0/90]_s$

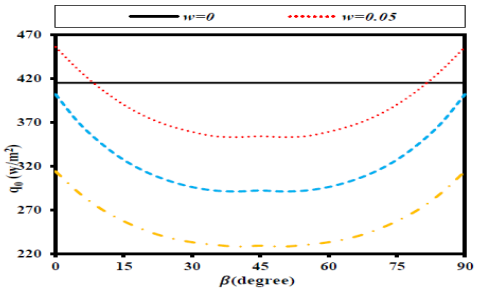

$[45/-45]_s$

$[30/-30]_s$

Fig.6
Effect of cutout rotation angle on the maximum allowable heat flux for different values of cutout bluntness.

Fig. 7 shows the effect of cutout aspect ratio on the maximum allowable heat flux of perforated Glass/epoxy laminates with different stacking sequences. As it was clear, the maximum allowable heat flux of laminate containing a quasi-square cutout decreased by increasing the aspect ratios of the cutout, so the strength of the laminate decreased. It was noteworthy that, in addition to the stacking sequence and the cutout orientation angle, the cutout aspect ratios have a significant effect on the values of the strength in laminated composite plates. It can be seen that the maximum value of the allowable heat flux for the stacking sequence of $[0/90]_s$ was equal to 397 w/m^2 at c =0.5 and β =25° and 155°. For the stacking sequence of $[45/-45]_s$, the maximum allowable heat flux was equal to 509 w/m^2 at c =0.5 and β =90°, while for the stacking sequence of $[30/-30]_s$, the maximum allowable heat flux was equal to 643 w/m^2 at c =0.5 and β =80° and 100°. The lowest maximum allowable heat flux was attained for the stacking sequences of $[0/90]_s$, $[45/-45]_s$ and $[30/-30]_s$ at β =40° and 140°, β =75° and 105°, and β =90° for c =2, respectively. Therefore, the values of cutout aspect ratio and the laminate stacking sequence as important parameters have significant effects on the maximum allowable heat flux of laminate.

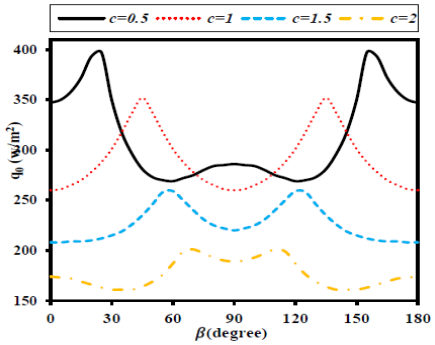

$[0/90]_s$

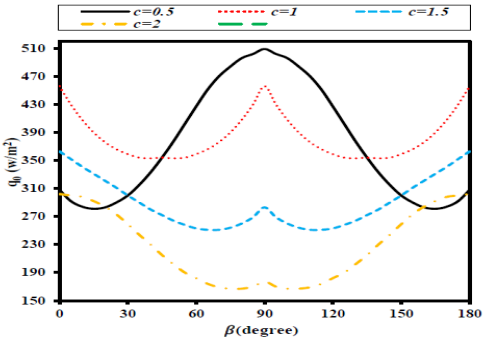

$[45/-45]_s$

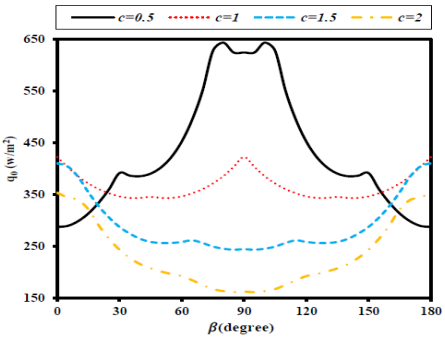

$[30/-30]_s$

Fig.7
Effect of rotation angle on the maximum allowable heat flux for different values of *c*.

4.1 Effect of heat flux angle

The effect of heat flux angle on the maximum allowable heat flux of the perforated laminated composite plate for different values of bluntness parameter (w) is illustrated in Fig. 8. As observed in the previous section, the maximum values of allowable heat flux for the stacking sequences of $[0/90]_s$, $[45/-45]_s$ and $[30/-30]_s$ were attained at β = 45°, β = zero or 90° and β = zero or 90°, respectively. Hence, in this section, these values are used to calculate the effect of heat flux angle on the maximum allowable heat flux. According to Tsai-Hill criteria, it was observed that the maximum allowable heat flux for the stacking sequence of $[0/90]_s$ for β = 45° was equal to 456 w/m^2 when δ = 45°, 135°, 225° and 315°. Moreover, for the stacking sequence of $[45/-45]_s$ at β = 0°, the maximum allowable heat flux was equal to 350 w/m^2 when δ = 0°, 90°, 180°, 270° and 360°, while, for the stacking sequence of $[30/-30]_s$ at β = 0°, the maximum allowable heat flux was equal to 422 w/m^2 when δ = 90° and 270°. It was noteworthy that the maximum value of the allowable heat flux was achieved in a non-circular cutout (w = 0.05). So, a circular cutout (w = 0) is not always an optimum shape of the cutout. According to the results of Fig. 8, the stacking sequence of laminate and heat flux angle play important roles in the values of the maximum allowable heat flux in the composite laminates containing a quasi-square cutout made of Glass/epoxy material.

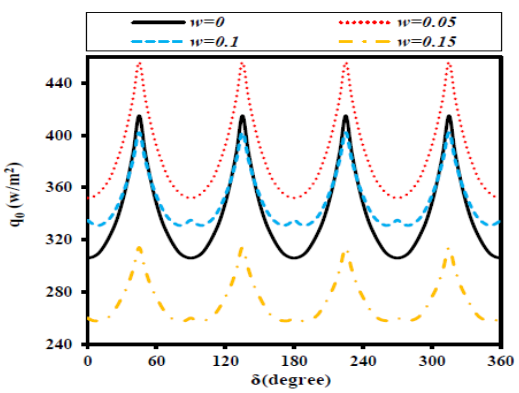

$[0/90]_s$

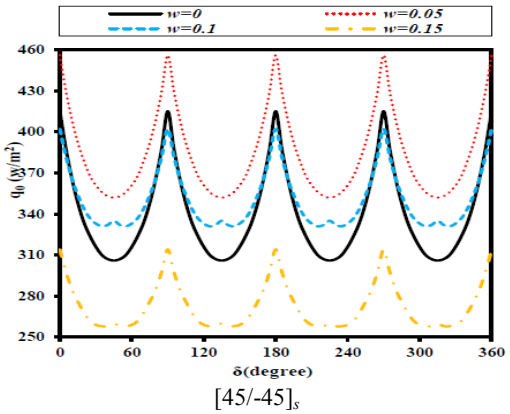

$[45/-45]_s$

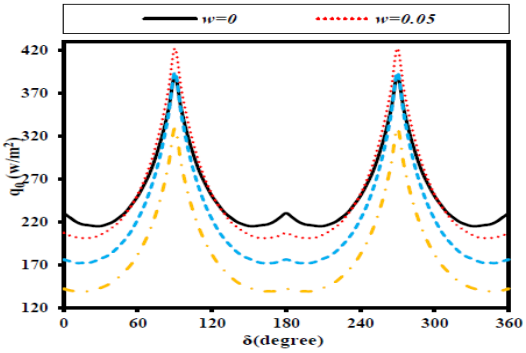

$[30/-30]_s$

Fig.8
Effect of flux angle on the maximum allowable heat flux in different values of w.

Fig. 9 shows the effect of heat flux angle on the maximum allowable heat flux of the symmetric laminated composite containing a quasi-square cutout with different cutout rotation angles. It was obtained that the maximum value of the allowable heat flux for the stacking sequence of $[0/90]_s$ was equal to 456 w/m^2 when δ = 45°, 135°, 225°, 315° and β = 45°, while that for the stacking sequence of $[45/-45]_s$ was equal to 456 w/m^2 when δ = 0°, 90°, 180°, 270°, 360° and β = 0°. For the stacking sequence of $[30/-30]_s$, the maximum value of allowable heat flux was equal to 422 w/m^2 at δ = 90°, 270° and β = 0°. The cutout orientation had a significant effect on the heat flux angle value for obtaining the maximum allowable heat flux value for the perforated symmetric laminated composite. As can be seen in Fig. 9, the location of the maximum allowable heat flux depends on the arrangement of the layers. It is clear that for the stacking sequence of $[0/90]_s$ by increasing the cutout orientation, the maximum value of allowable heat flux was increased. However, by changing the stacking sequence to $[45/-45]_s$ or $[30/-30]_s$ at β = 30° and β = 45° experienced a close-knit behavior. Therefore, in addition to β and δ, the stacking sequences play a key role in obtaining higher strength values for composite laminates under uniform heat flux.

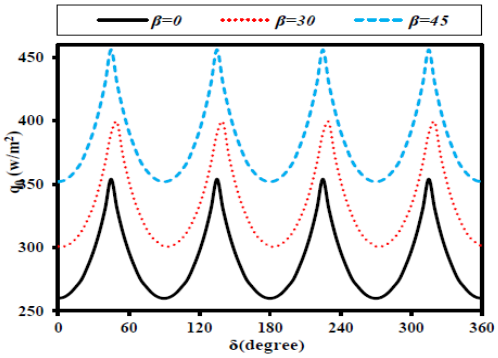

$[0/90]_s$

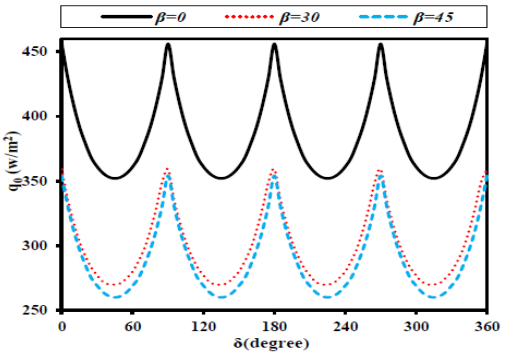

$[45/-45]_s$

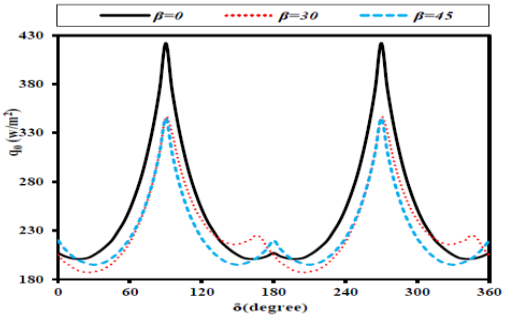

$[30/-30]_s$

Fig.9
Effect of flux angle on the maximum allowable heat flux in different values of β.

Fig. 10 shows the effect of heat flux angle on the maximum allowable heat flux of Glass/epoxy laminate with a quasi-square cutout with different cutout aspect ratios. It can be seen that the maximum value of the allowable heat flux for the stacking sequence of $[0/90]_s$ was equal to 509 w/m^2 when $\delta = 45°$, 225° and $c = 0.5$ and for the stacking sequence of $[45/-45]_s$ was equal to 509 w/m^2 when $\delta = 0°$, 180°, 360° and $c = 0.5$. For the stacking sequence of $[30/-30]_s$, the maximum allowable heat flux was equal to 422 w/m^2 at $\delta = 90°$, 270° and $c = 1$. It was noteworthy that, by changing the heat flux angle location, the maximum value of the allowable heat flux was changed. According to Fig. 10, for the stacking sequence of $[0/90]_s$, the highest strength was obtained at $c = 1$ when $\delta = 0°$ while by changing the heat flux angle location, the highest strength was obtained at $c = 0.5$ when $\delta = 45°$. This behavior was different for the stacking sequences of $[45/-45]_s$ and $[30/-30]_s$. Therefore, in addition to the stacking sequence, the cutout rotation angle and heat flux angle are important in achieving the maximum allowable heat flux. It should be noted that the results of Fig. 10 for the stacking sequences of $[0/90]_s$, $[45/-45]_s$ and $[30/-30]_s$ are presented with the assumptions of $w = 0.05$ and $\beta = 45^o$, $\beta = 0^o$ and $\beta = 0^o$.

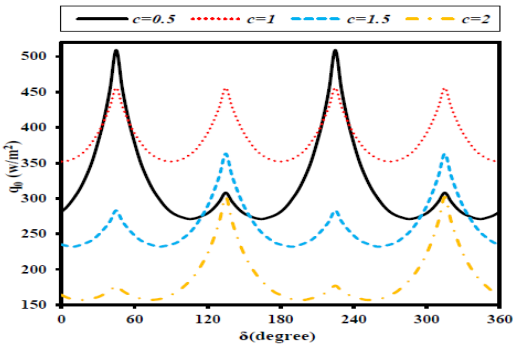

$[0/90]_s$

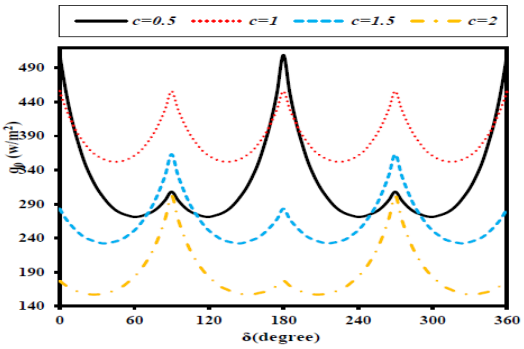

$[45/-45]_s$

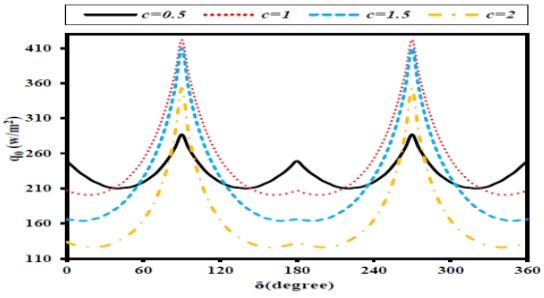

$[30/-30]_s$

Fig.10
Effect of flux angle on the maximum allowable heat flux in different values of c.

5 CONCLUSION

This paper examined the maximum allowable heat flux for the symmetric composite laminate containing a quasi-square cutout with different stacking sequences under uniform heat flux. The analytical solution was obtained based

on the thermoelasticity theory and by using the complex variable method. The stress function and conformal mapping function were utilized to determine the strength of a composite plate containing a non-circular cutout shape. The Tsai-Hill criterion was employed to study the maximum allowable heat flux of laminates with different staking sequence. Further, the effect of parameters including the cutout orientation angle, the heat flux angle, the cutout bluntness, the cutout aspect ratio and the laminate stacking sequence was investigated on the maximum allowable heat flux for Glass/epoxy symmetric laminated plates. The results showed that the laminate stacking sequence and the cutout geometrical parameters can considerably influence the maximum allowable heat flux of laminates with cutouts. Accordingly, by considering the proper laminate stacking sequence and proper values for the cutout orientation and heat flux angle, the maximum allowable heat flux can be increased. Also, the bluntness and the cutout aspect ratio parameters were other effective parameters involved in achieving higher maximum allowable heat flux. It was found out that for the laminates with the stacking sequences of $[0/90]_s$, $[45/-45]_s$ and $[30/-30]_s$ containing non-circular cutouts with a bluntness parameter of $w = 0.05$ located at angular positions of $\beta = 45°$, $\beta = 0°$ and $\beta = 0°$ and the heat flux angles of $\delta = 45°$, 135°, 225°, 315°, $\delta = 0°$, 90°, 180°, 270°, 360° and $\delta = 90°$, 270°, respectively, the maximum allowable heat flux were obtained. Therefore circle may not be the optimum shape of cutout. Finite element analyses were employed for validating the analytical solutions. There was a reasonable agreement between the finite element and analytical results.

REFERENCES

[1] Dai L., Chen Y., Wang Y., Lin Y., 2020, Experimental and numerical analysis on vibration of plate with multiple cutouts based on primitive cell plate with double cutouts, *International Journal of Mechanical Sciences* **183**: 105758.

[2] Kathiresan M., 2020, Influence of shape, size and location of cutouts on crashworthiness performance of aluminum conical frusta under quasi-static axial compression, *Thin-Walled Structures* **154**: 106793.

[3] Hussein O.S., Mulani S.B., 2018, Optimization of in-plane functionally graded panels for buckling strength: Unstiffened, stiffened panels, and panels with cutouts, *Thin-Walled Structures* **122**: 173-181.

[4] Muskhelishvili N., 1977, *Some Basic Problems of Mathematical Theory of Elasticity*, Netherlands, Noordhooff, Groningen, Holland.

[5] Lekhnitskii S.G., 1969, *Anisotropic Plates,* Gordon and Breach Science, New York.

[6] Florence A.L., Goodier J.N., 1959, Thermal stress at spherical cavities and circular holes in uniform heat flow, *Journal of Applied Mechanics* **26**: 293-394.

[7] Florence A.L., Goodier J.N., 1960, Thermal stresses due to disturbance of uniform heat flow by an insulated ovaloid hole, *Journal of Applied Mechanics* **27**: 635-639.

[8] Hasebe N., Wang X., 2005, Complex variable method for thermal stress problem, *Journal of Thermal Stresses* **28**: 595-648.

[9] Tarn J.Q., Wang Y.M., 1993, Thermal stresses in anisotropic bodies with a hole or a rigid inclusion, *Journal of Thermal Stresses* **16**: 455-471.

[10] Rezaeepazhand J., Jafari M., 2005, Stress analysis of perforated composite plates, *Composite Structures* **71**: 463-468.

[11] Jafari M., Bayati Chaleshtari M.H., 2017, Using dragonfly algorithm for optimization of orthotropic infinite plates with a quasi-triangular cut-out, *European Journal of Mechanics - A/Solids* **66**: 1-14.

[12] Ehsani A., Rezaeepazhand J., 2016, Stacking sequence optimization of laminated composite grid plates for maximum buckling load using genetic algorithm, *International Journal of Mechanical Sciences* **119**: 97-106.

[13] Huang J., Li C., Liu W., 2020, Investigation of internal friction and fracture fatigue entropy of CFRP laminates with various stacking sequences subjected to fatigue loading, *Thin-Walled Structures* **155**: 106978.

[14] Al-saadi A.U., Aravinthan T., Lokuge W., 2019, Effects of fibre orientation and layup on the mechanical properties of the pultruded glass fibre reinforced polymer tubes, *Engineering Structures* **198**: 109448.

[15] Wu Z., Zhang Q., Li B., Liu Y., Pan Z., 2020, Transverse impact response and residual flexure characteristics of braided composite tubes: Effect of stacking sequence, *Thin-Walled Structures* **155**: 106900.

[16] Wei R., Pan G., Jiang J., Shen K., Lyu D., 2019, An efficient approach for stacking sequence optimization of symmetrical laminated composite cylindrical shells based on a genetic algorithm, *Thin-Walled Structures* **142**: 160-170.

[17] Ukadgaonker V.G., Rao D.K.N., 2000, A general solution for stresses around holes in symmetric laminates under inplane loading, *Composite Structures* **49**: 339-354.

[18] Sharma D.S., 2015, Stresses around polygonal hole in an in finite laminated composite plate, *European Journal of Mechanics / A Solids* **54**: 44-52.

[19] Sharma D.S., 2016, Stresses around hypotrochoidal hole in infinite isotropic plate, *International Journal of Mechanical Sciences* **105**: 32-40.

[20] Mousanezhad Viyand D., Yazdani Sarvestani H., Nosier A., 2013, Stress analysis in symmetric composite laminates subjected to shearing loads, *International Journal of Mechanical Sciences* **75**: 16-25.

[21] Pang S.J., Zhou Y.T., Li F.J., 2018, Analytic solutions of thermoelectric materials containing a circular hole with a straight crack, *International Journal of Mechanical Sciences* **144**: 731-738.

[22] Kaczyński A., 2014, Thermal stress analysis of a three-dimensional anticrack in a transversely isotropic solid, *International Journal of Solids and Structures* **51**: 2382-2389.
[23] Dave J.M., Sharma D.S., 2018, Stress field around rectangular hole in functionally graded plate, *International Journal of Mechanical Sciences* **136**: 360-370.
[24] Rasouli M., Jafari M., 2016, Thermal stress analysis of infinite anisotropic plate with elliptical hole under uniform heat flux, *Journal of Thermal Stresses* **39**: 1341-1355.
[25] Chao C.K., Chen F.M., Lin T.H., 2017, Thermal stresses induced by a remote uniform heat flow interacting with two circular inclusions, *Journal of Thermal Stresses* **40**: 564-582.
[26] Chao C.K., Gao B., 2001, Mixed boundary-value problems of two-dimensional anisotropic thermoelasticity with elliptic boundaries, *International Journal of Solids and Structures* **38**: 5975-5994.
[27] Chaudhuri R.A., 2010, Transverse shear stress distribution through thickness near an internal part-through elliptical hole in a stretched plate, *Composite Structures* **92**: 818-825.
[28] Chaudhuri R.A., Seide P., 2010, Interlaminar shear stresses around an internal part-through hole in a laminated composite plate, *Composite Structures* **92**: 835-843.
[29] Nageswara Rao D.K., Ramesh Babu M., Raja Narender Reddy K., Sunil D., 2010, Stress around square and rectangular cutouts in symmetric laminates, *Composite Structures* **92**: 2845-2859.
[30] Zhou S., Sun Y., Chen B., Tay T.E., 2017a, Progressive damage simulation of open-hole composite laminates under compression based on different failure criteria, *Journal of Composite Materials* **51**: 1239-1251.
[31] Zhou S., Sun Y., Chen B., Tay T.E., 2017b, Material orthotropy effects on progressive damage analysis of open-hole composite laminates under tension, *Journal of Reinforced Plastics and Composites* **36**: 1473-1486.
[32] Patel N.P., Sharma D.S., 2019, An analytical investigation of the best stacking sequence of a symmetric laminated composite plate weakened by a hole, *Mathematics and Mechanics of Solids* **24**: 1387-1404.
[33] Tian K., Zhou S., Yang C., Zhang J., Zhou C., 2019, Tension failure simulation of notched composite laminate using floating node method combined with in-situ effect theory, *Journal of Materials Research and Technology* **8**: 2494-2507.
[34] Sharma D.S., Patel N.P., Trivedi R.R., 2014, Optimum design of laminates containing an elliptical hole, *International Journal of Mechanical Sciences* **85**: 76-87.
[35] Jafari M., Moussavian H., Chaleshtari M.H.B., 2018, Optimum design of perforated orthotropic and laminated composite plates under in-plane loading by genetic algorithm, *Structural and Multidisciplinary Optimization* **57**: 341-357.
[36] Jafari M., Jafari M., 2019, Thermal stress analysis of orthotropic plate containing a rectangular hole using complex variable method, *European Journal of Mechanics A/Solids* **73**: 212-223.
[37] Herakovich C.T., 1998, *Mechanics of Fibrous Composites*, Johan Wiley & Sons, University of Virginia, Virginia.
[38] Jafari M., Bayati Chaleshtari M.H., Ardalani E., 2018, Determination of optimal parameters for finite plates with a quasi-square hole, *Journal of Solid Mechanics* **10**(2): 300-314.
[39] Bayati Chaleshtari M.H., Khoramishad H., 2021, Effect of stacking sequence on thermal stresses in laminated plates with a quasi-square cutout using the complex variable method, *Structural Engineering and Mechanics* **77**(2): 245-259.